Relation between Molecular Structure and Flow Instability for Ethylene/α-olefin Copolymers.

Masayuki Yamaguchi, [1,2,*] Hiroshi Miyata,[2] Victor Tan,[1] Costas G. Gogos[1]

[1]Polymer Processing Institute
GITC Building, Suite 3901, New Jersey Institute of Technology, Newark, NJ 07102

[2]Yokkaichi Research Laboratory, TOSOH Corporation
1-8 Kasumi, Yokkaichi, Mie, 510-8540 Japan

Corresponding to
Masayuki Yamaguchi
TOSOH Corporation, Yokkaichi Research Laboratory, 1-8 Kasumi, Yokkaichi, Mie, 510-8540 Japan
(phone) +81-593-63-4174; (fax) +81-593-63-2641; (e-mail) m_yama@tosoh.co.jp

abstract

Surface instabilities in a capillary extrusion have been studied for various ethylene/α-olefin copolymers. It is found that the onset stress of shark-skin failure for ethylene/1-hexene copolymer (EHR) decreases rapidly with increasing 1-hexene content, whereas that of ethylene/propylene copolymer (EPR) is independent of propylene content in the experimental region. Consequently, EHR with high 1-hexene content exhibits shark-skin at low stress level compared to EPR. Lower rubbery plateau modulus, leading to higher Deborah number at the same stress level, is attributed to the lower onset stress. Further, the low entanglement density will cause cracks at lower stress level like glassy polymers, which is also responsible for the low onset stress for shark-skin.

Keywords;

polyolefins; extrusion; rheology

Introduction

Recent development of metallocene catalyst technology makes it possible to produce a tailored ethylene/α-olefin copolymer at a commercial scale. As a result, there is a growing great interest in the relation between molecular structure and various kinds of properties, such as thermal, rheological, and mechanical properties,[1-6] which gives us information on "molecular design". To the best of our knowledge, however, the effect of molecular structure, especially the species and content of α-olefin unit in copolymers, on flow instabilities has not been clarified yet, although it is very important from the industrial point of view. Further, since metallocene polymers have a narrow molecular weight distribution compared to a conventional polyolefin by Zieglar-Natta catalyst, flow instabilities often take place early, and limit the production speed.

It has been generally accepted that flow instabilities can be roughly classified as follows;[7] (1) Surface instabilities occurred at the die exit, such as shark-skin and slip-stick, and (2) Gross volumetric melt fracture due to the instability in the entrance of die, which is associated with long time relaxation mechanism, *i.e.*, melt elasticity.[8-10] In the case of ethylene/α-olefin copolymers with narrow molecular weight distribution, the former one, surface instabilities at the die exit, are more apt to be the course of the problem. Although the mechanism of surface instabilities has been studied for a long time based on the experimental results, as is well known, controversies still continue to be discussed.

Cogswell proposed that the origin of shark-skin is the crack created by the high level of tensile stress applied in the vicinity of the die exit,[11] which has been elucidated by optical and microscopic methods[12-16] and numerical modeling.[17,18] Further, it was also supported from experimental results that rheological properties under elongational flow, such as melt strength and strain hardening behavior, affect the onset of shark-skin.[15,19] Finally, Gogos et al. proposed possible methods to mitigate the shark-skin failure based on this mechanism.[16] Another well-known mechanism leading to the shark-skin is the slippage, *i.e.*, adhesive failure, between a polymer melt and the die

wall.[20-23] Since it is generally accepted that a high viscous polymer melt can slip on the wall,[24] the slippage may be the origin of surface instability, especially slip-stick failure, in some cases. Furthermore, Brochard and de Gennes proposed the molecular theory, in which disentanglement between bulk polymer chains and the polymer chains adhered on the wall, *i.e.*, cohesive failure, is the origin of surface instability.[25]

The role of entanglement couplings, which dominate rheological properties of polymer melts, however, has not been discussed to a great degree,[14,26] besides the theory proposed by Brochard and de Gennes[25] and some experimental studies[27,28] based on their theory.

In this study, we have investigated the flow instability for ethylene/propylene copolymers (EPR) and ethylene/1-hexene copolymers (EHR) with various amounts of α-olefin unit, and explored and discussed the critical stress for the onset of shark-skin. Further, molecular characteristics of the copolymers, such as average molecular weight between entanglement couplings, have been also clarified. The obtained result will give us a clue to point out to the mechanism of shark-skin from a viewpoint of molecular dynamics.

Experimental

Materials and Blend Preparation

The ethylene/propylene copolymer (EPR) and ethylene/1-hexene copolymer (EHR) employed were synthesized by a metallocene catalyst. The details in the molecular characteristics and polymerization methods were described in reference 6. Table 1 summarized the molecular weight, which were determined from combination measurements of intrinsic viscosity (VISCOTEK, Differential Viscometer Model 100) and gel permeation chromatography (Waters, 150-C) in ortho-dichlrobenzene at 135 ºC, and α-olefin content determined from ^{13}C nuclear magnetic resonance. The nomenclature of the samples used is as follows: *e.g.*, EPR37 is an ethylene/propylene copolymer whose

propylene content is ca. 37 mol%. All copolymers except EHR18 are fully amorphous at room temperature because of less ethylene sequence. Further, it was found from a differential scanning calorimetry measurement that the melting point of EHR18 is around 36 °C.

An Instron capillary rheometer was used for the evaluation of flow instabilities in a capillary extrusion. The extrusion was carried out at 70 and 160 °C. A tungsten carbide die of L/D = 33.2, D = 1.535 mm, and entrance angle = 90º was employed. The Bagley and Rabinowitsch corrections were not carried out, since L/D is large enough to neglect the end effect. Further, in order to eliminate polymer materials in the capillary, we washed the die prior to each measurement by xylene.

Oscillatory shear moduli, such as shear storage modulus G' and loss modulus G'', were measured at various temperatures using a parallel-plate rheometer (Rheometrics, RMS-800). The time-temperature superposition was applied to frequency dependence of oscillatory modulus at different temperatures.

Results

Linear Viscoelastic Properties

Figure 1 exemplifies the master curves of oscillatory shear moduli for EPR67 at 25 °C. The curves show the terminal and rubbery plateau zones in the reduced angular frequency ωa_T range. The value of rubbery plateau modulus G_N^0 can be determined by:[29]

$$G_N^0 = \frac{2}{\pi}\int_{-\infty}^{a} G'' d\ln\omega \qquad (1)$$

where a is the upper limit before the transition zone is entered.

In general, the parameter can be obtained by the integration of G'' over ln ω

encompassing the maximum of G''. In this study, the G'' versus ln ω curve was numerically integrated from ln ω = -∞ to the maximum of G'', and the result was doubled. Table 2 shows G_N^0 for the samples employed, in which some results were shown in the previous paper with the master curves.[6] Because of crystallization, master curves do not cover enough frequency scale to evaluate G_N^0 for EHR18. As seen in the table, G_N^0 decreases with increasing α-olefin content. Further, EHR exhibits a significantly lower G_N^0 than the EPR having the same α-olefin content in mole percent. As a result, G_N^0 of EPR37 is three times as much as that of EHR51. Some authors[6] made it clear that the rubbery plateau modulus G_N^0 of ethylene/α-olefin copolymers is simply expressed by the following equation based on the theory proposed by Graessley and Edwards.[30]

$$G_N^0 = K\left(m_0/14\right)^{-2.3} \tag{2}$$

$$m_0 = 14\left(1-x\right)+kx \tag{3}$$

where K the G_N^0 for linear polyethylene, m_0 the average molecular weight per main chain bond, x the mole fraction of copolymer and k the half of the molecular weight of α-olefin unit.

It is seemed that the results in Table 2 also agree with the above equations.

Capillary Extrusion

Figure 2 shows apparent wall shear stress σ plotted against apparent wall shear rate $\dot{\gamma}$ at 70 and 160 °C. The solid line represents the values calculated from linear viscoelastic behavior by the Cox-Merz empirical rule.[31] Further, the arrow indicates the point which shark-skin takes place. It is found that the predicted lines agree with experimental data even though shark-skin takes place, indicating that slip velocity, if present, is negligible. Moreover, there is no sharp change in the slope of flow curves in

this experiment. As seen in the figure, the slope of shear stress decreases with increasing 1-hexene content for EHRs, whereas EPR67 has a similar slope as EPR37. Further, the copolymer with high α-olefin content shows a larger shift factor irrespective of α-olefin species. Moreover, it is found that the critical shear stress for the onset of shark-skin, σ_c, at 160 ºC is higher than that at 70 ºC for all samples, which corresponds with the results of previous studies.[11,14,15,17-19,27]

Figure 3 shows extrudates of EHR18 obtained at 70 ºC. As seen in the figure, smooth, gloss surface is observed at 6.81 x 10^{-1} sec^{-1} (Figure 3(a)) and shark-skin is detected by naked eyes at 1.36 sec^{-1} (Figure 3(b)). Thus, the onset stress is between 9.7 x 10^4 Pa at $\dot{\gamma}$ =6.81 x 10^{-1} sec^{-1} and 1.41 x 10^5 Pa at 1.36 sec^{-1}. Increasing shear rate, the periodic distortion with small amplitude appears markedly as shown in Figures 3(c) and (d). After showing pine cone shape (Figures 3(d) and (e)), gross, chaotic, and volumetric melt fracture takes place at higher shear rate (Figure 3(g)). As shown in the figure, it is difficult to differentiate between the region of shark-skin and that of gross melt fracture. All EHRs exhibit similar behavior as EHR18 irrespective of extrusion temperature.

Figure 4 shows extrudates of EPR37 at 70 ºC. Shark-skin starts appearing at 2.04 sec^{-1} and 1.54 x 10^5 Pa, suggesting that the onset stress of EPR 37 is at the same level as that of EHR18. The amplitude of the periodic distortion increases with shear rate, and screw-type distortion appears as shown in Figure 4(d). Further, the screw-type distortion and smooth surface appear alternatively at 3.41 x 10 sec^{-1} (Figure 4(e)). Then, smooth surface appears again at relatively higher shear rate (Figure 4(f)), which is observed also for EPR67 at 70 ºC but not at 160 ºC. After smooth surface, the region of gross melt fracture takes place at higher shear rate, as shown in Figure 4(g). Because of the existence of smooth surface region at relatively high shear rate, the critical shear stress for the onset of gross melt fracture is also identified at 70 ºC; 4.45 x 10^5 Pa for EPR37 and 4.04 x 10^5 Pa for EPR67. At 160 ºC, however, smooth surface does not appear at higher shear rate after shark-skin failure. Therefore, it is impossible to evaluate the onset stress for gross melt fracture.

Figure 5 shows the relation between the onset stress of shark-skin σ_c at 160 ºC and α-olefin content in the copolymers. It is found that the onset stresses of EPRs and EHR18 are similar to that for metallocene HDPE reported by Vega et al.[32] Furthermore, σ_c decreases rapidly with 1-hexene content in EHR, whereas both EPRs show similar level. The figure demonstrates that EHR with high 1-hexene content exhibits the shark-skin failure at lower level of the wall stress.

Discussion

We ascribe the difference in σ_c between EPR and EHR to the difference in the density of entanglement couplings ν_e, because G_N^0, which is proportional to ν_e (equation (4)), is significantly dependent on the species and content of α-olefin unit in the copolymer.

$$\nu_e = \frac{\rho}{M_e} = \frac{G_N^0}{RT} \tag{4}$$

where M_e is the average molecular weight between entanglement coupling points.

As shown in Table 2, EPR has a high G_N^0, even though propylene content is high. On the other hand, G_N^0 of EHR falls off sharply with 1-hexene content.[6] This result demonstrates that EHR with high 1-hexene content exhibits a quite low G_N^0, *i.e.*, low density of entanglement couplings. According to El Kissi and Piau, the onset stress slightly decreases with the number of entanglement couplings per a chain,[14] which has been supported by the experiments employing various samples with different molecular weight.[26] Table 2 also shows the values of ν_e at 160 °C and M_w / M_e calculated by

equations (2) and (4) in order to avoid an experimental error. As seen in the table, however, the number of entanglement points per a chain seems to have no/less relation with the onset stress.

In Figure 6, the experimental onset stress σ_c, which is shown in Figure 5, is plotted against ν_e. As seen in the figure, σ_c increases with ν_e, irrespective of the species of α-olefin unit in the copolymers, suggesting that the entanglement density is related to the onset stress of shark-skin. This result demonstrates that a polymer having a low ν_e, *i.e.*, low G_N^0, shows shark-skin failure at low stress levels. Let us consider the effect of G_N^0 on the rheological properties under steady-state shear flow.

As is well known, the generalized Newtonian fluid (GNF) representation of the wall shear stress $\sigma(\dot{\gamma})$ is given by

$$\sigma(\dot{\gamma}) = \eta(\dot{\gamma})\dot{\gamma} \tag{5}$$

According to the Carreau GNF equation,[33] shear viscosity in the non-Newtonian region $\eta(\dot{\gamma})$ is expressed by

$$\eta(\dot{\gamma}) = \eta_0\left[1 + (\tau_w\dot{\gamma})^2\right]^{\frac{n-1}{2}} \tag{6}$$

where η_0 the zero-shear viscosity, n (<1) the constant which is the function of molecular weight distribution, and τ_w the weight-average relaxation time given by equation (7).

$$\tau_w \equiv \frac{\int \tau^2 H(\tau) d\ln\tau}{\int \tau H(\tau) d\ln\tau} = \eta_0 J_e^0 \tag{7}$$

where $H(\tau)$ the relaxation spectrum and J_e^0 the steady-state shear compliance.

The τ_w is replaced by the lower-order, number average relaxation time, τ_n, defined by,

$$\tau_n \equiv \frac{\int \tau H(\tau) d\ln\tau}{\int H(\tau) d\ln\tau} = \frac{\eta_0}{G_N^0} \tag{8}$$

Therefore,

$$\frac{\tau_w}{\tau_n} = \frac{J_e^0}{J_N^0} = f \tag{9}$$

where f (>1) the constant which is the function of molecular weight distribution,[29] and $J_N^0 = 1/G_N^0$.

Consequently, the wall shear stress $\sigma(\dot{\gamma})$ is represented by

$$\sigma(\dot{\gamma}) = \dot{\gamma}\eta_0 \left[1 + f^2(\tau_n\dot{\gamma})^2\right]^{\frac{n-1}{2}} \tag{10}$$

Further, equation (10) can be expressed using Deborah number, $De\,(=\tau_n\dot{\gamma})$, and G_N^0 as,

$$\sigma(\dot{\gamma}) = De\, G_N^0 \left[1 + f^2(De)^2\right]^{\frac{n-1}{2}} \tag{11}$$

Since f is usually considerably larger than 1, *i.e.*, $1 << f^2(De)^2$,

$$\sigma(\dot{\gamma}) \cong f^{n-1}(De)^n G_N^0 \tag{12}$$

Equation (12) demonstrates that a polymer with lower G_N^0, *i.e.*, lower ν_e, shows a higher De at the same level of the wall stress, which may explain the result of Figure 6. It is generally accepted that a polymer stores more energy during flow at high De conditions, and thus behaves like a solid material. As a result, slip or crack, which will be the origin of shark-skin failure as mentioned below, takes place for a polymer melt.[24] Further, the equation also explains that a polymer with narrow molecular weight distribution, *i.e.*, having a small f, is easy to exhibit surface instabilities.

Hereafter, we will discuss the mechanism of the shark-skin failure from the molecular point of view. When the debonding stress between the wall and a polymer melt is less than the cohesive strength of the polymer melt, the polymer slips on the wall at levels of the wall shear stress higher than the debonding stress. If the slip does not take place constantly, it will lead to surface instabilities such as slip-stick failure. However, in many cases, as pointed out by Venet and Vergnes,[18] adhesive failure may not be the main origin of, at least, shark-skin instability. As discussed extensively in recent studies,[15,16,18,19] some form of the crack mechanism, originally proposed by Cogswell,[11] is becoming to be more accepted as the probable origin of shark-skin instability, although there is still possibility that slip or other mechanism is responsible for shark-skin in some cases. Further, Cogswell also indicated that the discontinuity of velocity at the die exit wall region, leading to elongational wall velocity acceleration and tensile stresses, is responsible for the cracks,[11] which eventually may appear like a "peel-off" failure.[16] The stress at the crack-opening can be discussed referring to the failure mechanism of glassy amorphous polymers,[34-37] because of the high Deborah number at the prevailing flow conditions as mentioned above. According to Kausch,[35] localized decohesion of molecular coils, which takes place in the region with less degree of entanglement couplings, is the primary step of microvoids leading to a macroscopic crack through crazing. As a result, cracks are easily generated in polymers with less

entanglement density. The relationship between entanglement density ν_e and the critical stress for crazing, the precursor of the crack, σ_b , has been studied both theoretically[36,38] and experimentally.[38,39] According to them, σ_b falls off rapidly with increasing ν_e . Turning to Figure 6, we observe a strikingly similar strong dependence of the onset stress σ_c (at the capillary wall) to ν_e of the samples employed. In examining this similarity, we may conclude that in the case of the extrusion at higher elastic, *i.e.*, higher Deborah number, conditions, the origin of instability will be the cracking of the "elastic" melt on the surface above σ_c. Further, the propagation of these surface cracks on the extrudate emerging from the capillary, which will also be facilitated by lower ν_e, will be responsible for the shark-skin topography. Moreover, it has been generally accepted that σ_b slightly decreases with increasing temperature,[39-41] which corresponds with the onset stress for shark-skin instabilities.

Conclusions

Flow instabilities in a capillary extrusion have been investigated employing various ethylene/α-olefin copolymers with narrow molecular weight distributions. In this study, we focused on the effect of the species and content of α-olefin unit in the copolymers. It was found that the critical stress for the onset of shark-skin failure for EHR decreases monotonically with increasing 1-hexene content, whereas EPR with 67 mol% of propylene exhibits a similar level of the onset stress as EPR with 37 mol% of propylene. As a result, the EHR with high 1-hexene content exhibits shark-skin instabilities even at low shear stress. Further, the onset stress decreases with increasing the average molecular weight between entanglement couplings. Having low rubbery plateau modulus, which leads to high Deborah number at the same stress level, will be one of the reasons for the

low level of the onset stress for EHR with high 1-hexene content. Furthermore, the relationship between the onset stress and the entanglement density is well explained following the fracture mechanism of glassy amorphous polymers qualitatively.

Moreover, shark-skin starts appearing at lower stress level when the extruded melt temperature is high, irrespective of the molecular structure, which is also explained by the fracture mechanism of glassy polymers. In the case of EPR at 70 ºC, smooth surface appears again at higher stress region than the onset stress of shark-skin failure. On the other hand, smooth surface is observed only in the lower shear rate region for EHR.

References

1. Carella J, Graessley WW, Fetter LJ. Macromolecules 1984;17:2775.
2. Vega JF, Santamaria A, Minoz-Escalona A, Lafuente P. Macromolecules 1998;31:3639.
3. Lohse DJ, Graessley WW. in Polymer Blends, Eds Paul DR, Bucknall CB. Chap. 8, Wiley-Interscience, New York, 1999.
4. Yamaguchi M. Dissertation (Structure and Properties for Binary Blends of Polypropylene and Ethylene─α-olefin copolymers), Kyoto University, Kyoto, Japan 1999.
5. Mäder D, Heineman J, Walter P, Mülhaupt R. Macromolecules 2000;33:1254.
6. Miyata H, Yamaguchi M, Akashi M. Polymer 2001;42:5763.
7. Tordella JP. in Rheology, Ed Erich FR. Academic Press, New York, p.57, 1969.
8. White JL, Appl Polym Symp 1973;20:155.
9. Yamaguchi M. J Appl Polym Sci 2001;82:1277.
10. Yamaguchi M, Todd DB, Gogos CG. Adv Polym Technol submitted.
11. Cogswell FN. J Non-Newtonian Fluid Mech 1977;2:37.
12. Sornberger G. Quantic JC, Fajdle B, Vergnes JF, Agassant JF. J Non-Newtonian Fluid Mech 1987;23:123.
13. Beaufils P, Vergnes B, Agassant JF. Intern Polym Proc 1989;4:78.
14. El Kissi N, Piau JM. in Rheology for Polymer Melt Processing, Eds. Piau JM, Agassant JF. Elservier Science, 1996.
15. Venet C, Vergnes B. J Rheol 1997;41:873.
16. Gogos CG, Qian B, Todd DB, Veariel TR. Preceeding of ANTEC 2002, San Francisco, CA, 2002.
17. Tanner RI. Engineering Rheology, Oxford Univ Press, New York, 1985.
18. Venet C, Vergnes B. J Non-Newtonian Fluid Mech 2000;93:117.
19. Rutgers R, Mackley M. J Rheol 2000;44:1319.
20. Blyer LL, Hart AC. Polym Eng Sci 1970;10:193.
21. Ramamurthy AV. J Rheol 1986;30:337.

22. Kalika DS, Denn MM. J Rheol 1987;31:815.
23. Ghanta VG, Riise BL, Denn M. J Rheol 1999;43:435.
24. Larson RG. The Structure and Rheology of Complex Fluids, Oxford University Press, New York, 1988.
25. Brochard F, de Gennes PG. Langmuir 1992;8:3033.
26. Vlachopoulos J, Alam M. Polym Eng Sci 1972;12:184.
27. Wang SQ, Drda PA. Macromolecules 1996;29:2627, 4115.
28. Hatzikiriakos SG, Kazatchkov IB, Vlassopoulos D. J Rheol 1997;41:1299.
29. Ferry JD. Viscoelastic Properties of Polymers, Third Ed, Wiley, New York, 1980.
30. Graessley WW, Edwards SF. Polymer 1981;22:1329.
31. Cox WP, Merz EH. J Polym Sci 1958;28:619.
32. Vega JF, Minoz-Escalona A, Santamaria A, Munoz ME, Lafuente P. Macromolecules 1996;29:960.
33. Carreau PJ. Ph.D. thesis, Univ. Wisconsin, 1968.
34. Kambour RP. J Polym Sci Macromolecular Review 1973;7:1.
35. Kausch HH, Polymer Fracture, Chapter 9, Springer-Verlag, Berlin, 1978.
36. Kramer EJ, Berger LL. Adv Polym Sci 1990;91/92:1.
37. Estevez R, Tijssens MGA, Van der Giessen E. J Mech Phys Solids 2000;48:2585.
38. Wu S. Polym Eng Sci 1990;30:753.
39. Yamamoto T, Furukawa H. Polym 1995;36:2393.
40. Ishikawa M, Ogawa H, Narisawa I. J Macromol Sci Phys 1977;15:1791.
41. Ishikawa M, Ogawa H. J Macromol Sci Phys 1981;19:421.

Table 1 Characteristics of polymers

sample	α-olefin		molecular weight	
	species	Content (mol%)	M_n x 10^{-4}	M_w x 10^{-4}
EPR37	propylene	37.2	7.0	10
EPR67	propylene	66.7	9.0	14
EHR18	1-hexene	18.2	13	23
EHR33	1-hexene	32.5	13	23
EHR40	1-hexene	39.8	15	25
EHR51	1-hexene	50.5	14	23

Table 2 Rubbery plateau modulus G_N^0, entanglement density ν_e, and number of entanglement couplings per a chain M_w / M_e

sample	G_N^0 (MPa) (exp.)	ν_e (mol/m^3) (calc.)	M_w / M_e (calc.)
EPR37	1.06	315	53.8
EPR67	0.88	240	56.9
EHR18	—	229	89.1
EHR33	0.42	148	58.1
EHR40	0.44	121	50.9
EHR51	0.31	93.6	37.1

Figure Captions

Figure 1 Master curves of oscillatory shear moduli at 25 ºC for EPR67.

Figure 2 Flow curves at 70 and 160 ºC for (a) EPR37, (b) EPR67, (c) EHR18, (d) EHR33, (e) EHR40, (f) EHR51. The arrows indicate the point which shark-skin start appearing, and the solid lines are the calculated shear stress from oscillatory shear modulus.

Figure 3 Extrudates of EHR18 at 70 ºC. Shear rates are (a) 1.36 sec^{-1}, (b) 2.72 sec^{-1}, (c) 6.81 sec^{-1}, (d) 1.36×10^{1} sec^{-1}, (e) 3.41×10^{1} sec^{-1}, (f) 6.81×10^{1} sec^{-1}, (g) 1.36×10^{2} sec^{-1}.

Figure 4 Extrudates of EPR37 at 70 ºC. Shear rates are (a) 6.81×10^{-1} sec^{-1}, (b) 1.36 sec^{-1}, (c) 3.41 sec^{-1}, (d) 6.81 sec^{-1}, (e) 1.36×10^{1} sec^{-1}, (f) 3.41×10^{1} sec^{-1}, (g) 6.81×10^{1} sec^{-1}.

Figure 5 Relation between onset stress for shark-skin σ_c at 160 ºC and the content of α-olefin unit in the copolymers.

Figure 6 Relation between ν_e and σ_c at 160 ºC.

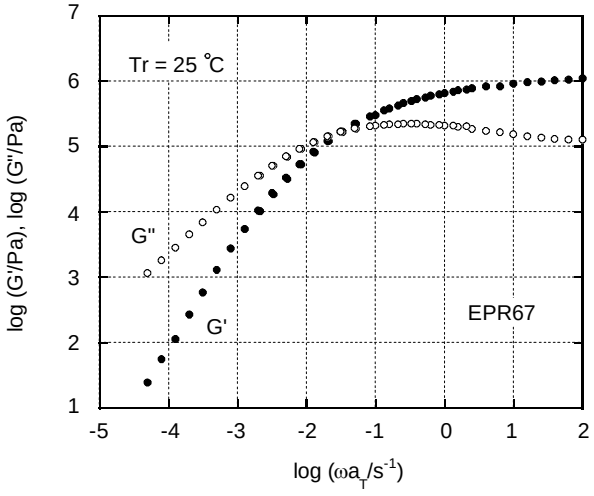

Yamaguchi, Figure 1

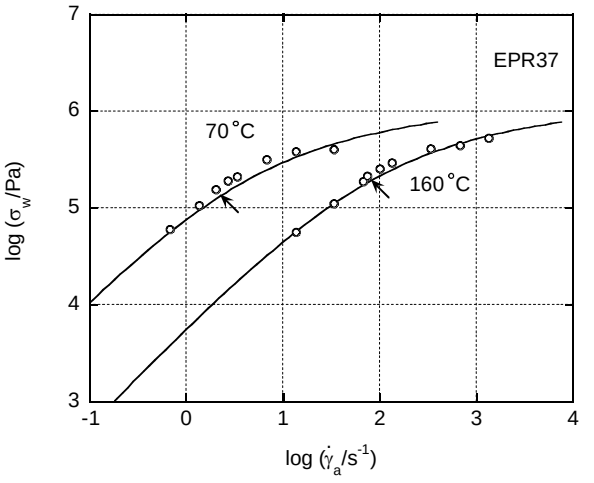

Yamaguchi, Figure 2(a)

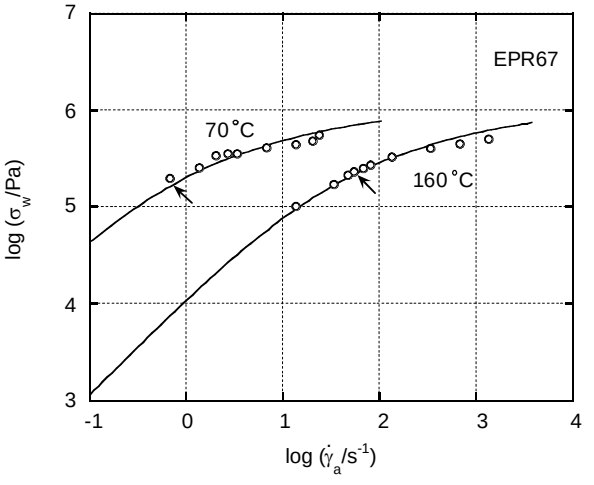

Yamaguchi, Figure 2(b)

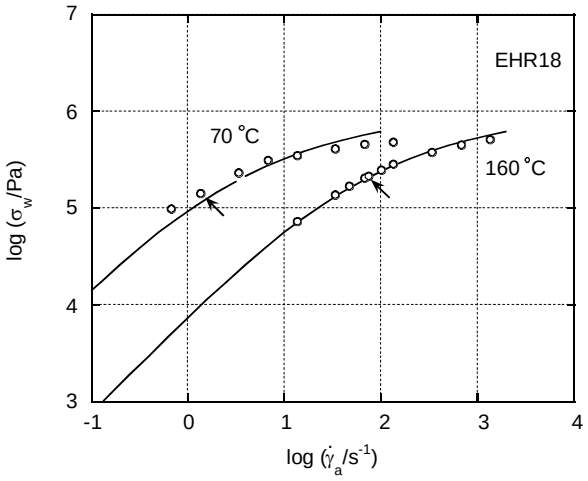

Yamaguchi, Figure 2(c)

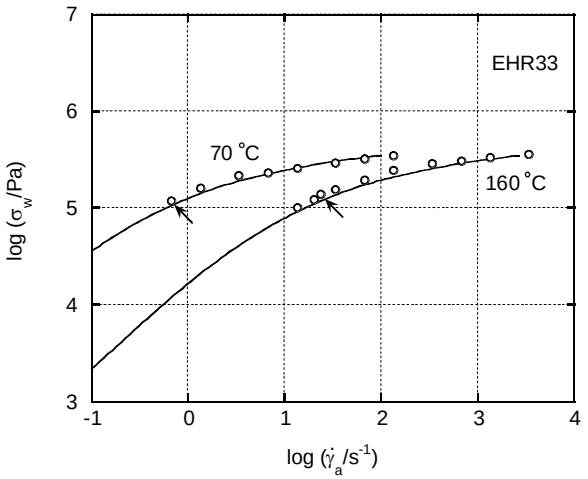

Yamaguchi, Figure 2(d)

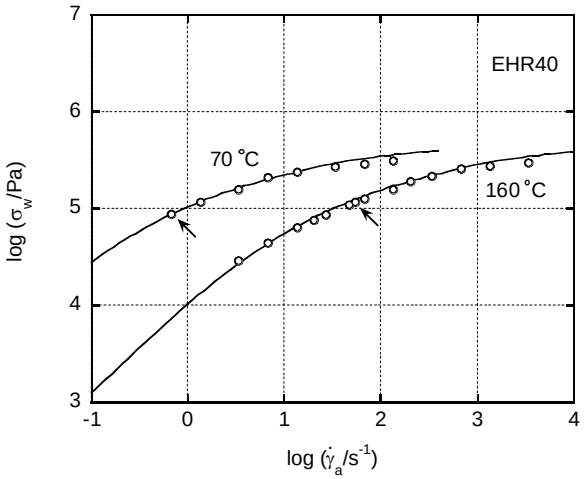

Yamaguchi, Figure 2(e)

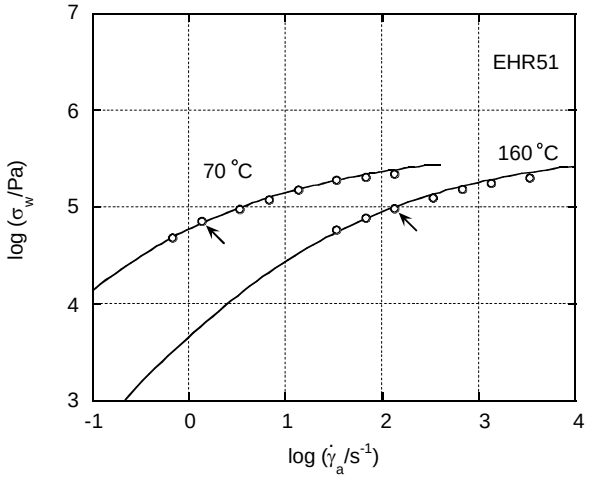

Yamaguchi, Figure 2(f)

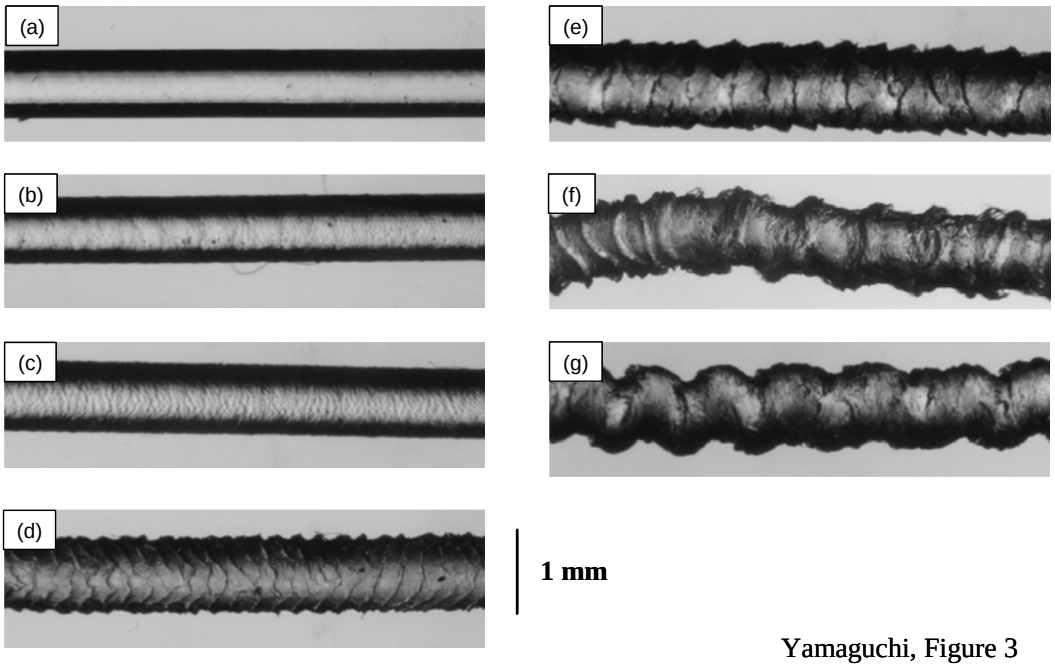

Yamaguchi, Figure 3

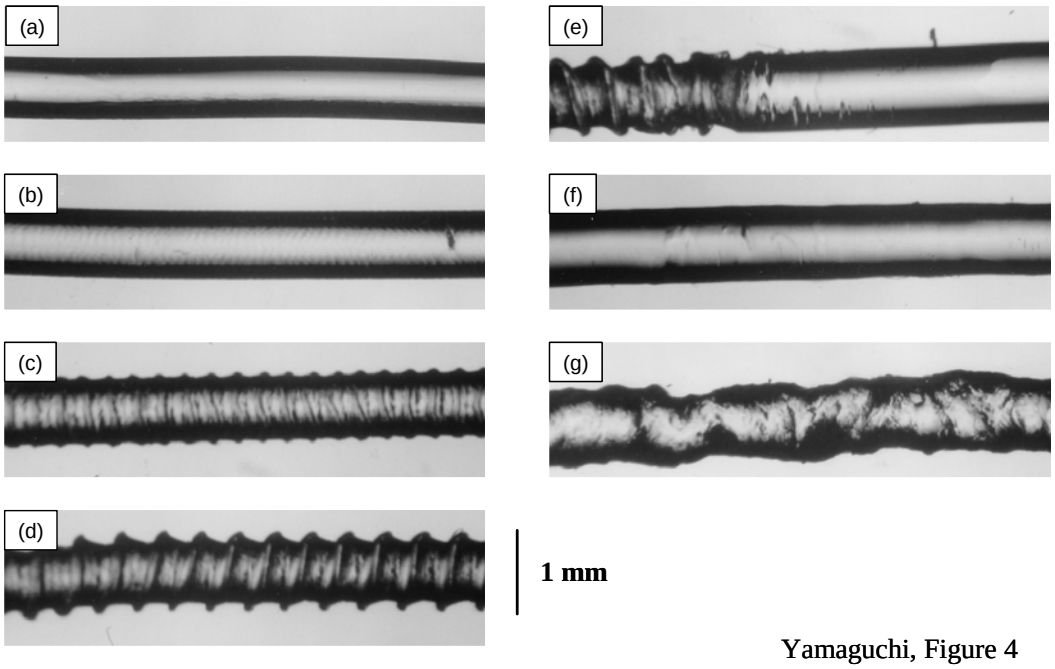

Yamaguchi, Figure 4

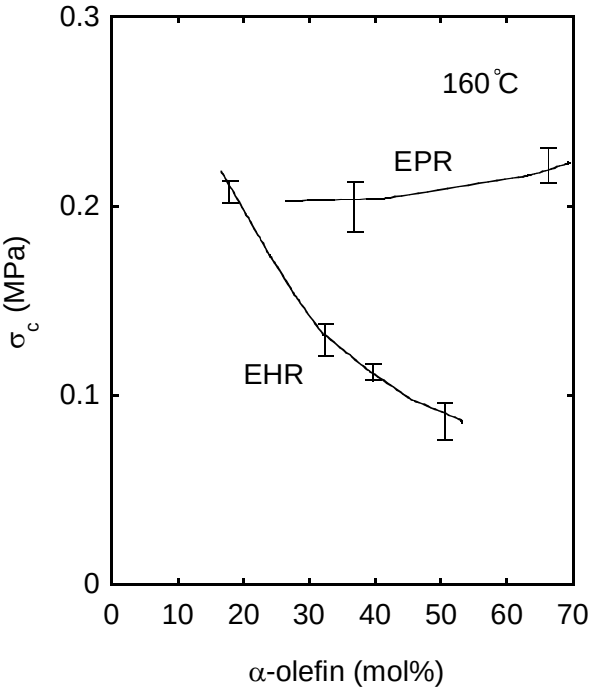

Yamaguchi, Figure 5

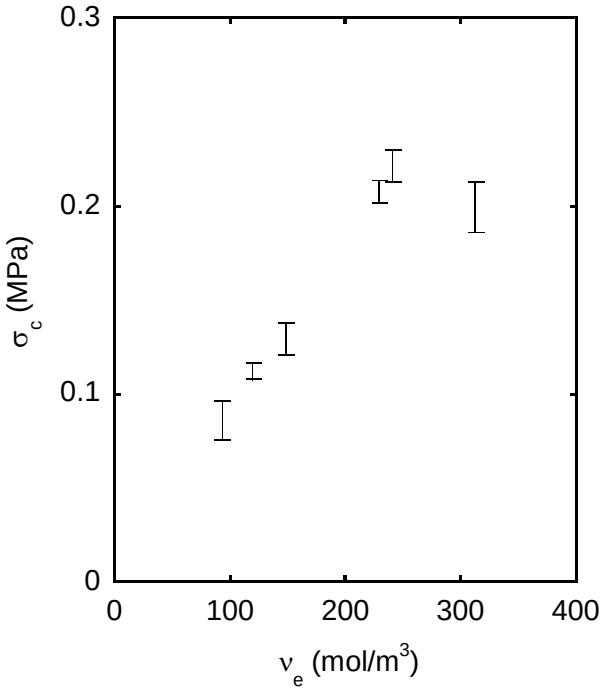

Yamaguchi, Figure 6